Deoxydehydration of glycerol to allyl alcohol catalysed by ceria-supported rhenium oxide

Karen Silva Vargas, Jeremie Zaffran, Marcia Araque, Masahiro Sadakane, Benjamin Katryniok

Molecular Catalysis 535 (2023) 112856

Contents lists available at ScienceDirect

Molecular Catalysis

journal homepage: www.journals.elsevier.com/molecular-catalysis

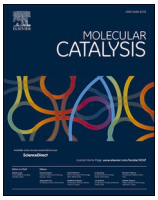

Deoxydehydration of glycerol to allyl alcohol catalysed by ceria-supported rhenium oxide

Karen Silva Vargas [a], Jeremie Zaffran [b], Marcia Araque [b], Masahiro Sadakane [c], Benjamin Katryniok [b,*]

[a] Ecole de Biologie Industrielle - EBI, UPR EBInnov®, 49 Avenue des Genottes CS90009 95895, Cergy-Pontoise, France
[b] Univ. Lille, CNRS, Centrale Lille, ENSCL, Univ. Artois, UMR 8181 - UCCS - Unité de Catalyse et Chimie du Solide, F-59000 Lille, France
[c] Department of Applied Chemistry, Faculty of Engineering, Hiroshima University, Hiroshima, Japan

A B S T R A C T

The Deoxydehydration (DODH) of glycerol to allyl alcohol was studied over ceria-supported rhenium oxide catalyst. Mesoporous ceria materials were synthetized via a nanocasting process using SiO_2 and activated carbon as hard templates. The as-obtained ceria supports were impregnated with 2.5-10 wt.% ReO_x and applied in the DODH reaction of glycerol to allyl alcohol at 175°C in batch conditions using 2-hexanol as solvent and hydrogen donor. As the characterisations revealed that the template removal was a critical step in the synthesis of the mesostructured ceria via the nanocasting method, the influence of the presence of the hard template was studied in detail by comparison to commercial ceria supports. The catalyst based on the nanocasting ceria showed higher performance of up to 88% yield in allyl alcohol and was reusable for 3 cycles without reactivation step. No evidence of leaching was observed via hot filtration test. The characterisation of the catalyst by XPS revealed the presence of Re^{4+} species after test, which led us propose that two redox couples, namely Re^{7+}/Re^{5+} and Re^{6+}/Re^{4+}, are involved during DODH of glycerol to allyl alcohol, which was further confirmed by DFT calculations.

1. Introduction

Due to the declining petroleum resources, the utilization of renewable alternatives such as biomass has gained increased attention notably with the growing demand for sustainable production of chemicals. In difference to petrol derived chemical, biomass derived molecules are highly functionalized, whereby reduction of the oxygen content is required to obtain value-added chemicals [1–3]. Hereby, olefinic compounds are an attractive target since they are important platform chemicals, which today are still produces primarily from petroleum resources [1,4,5]. Allyl alcohol is a promising platform molecule due to its broad range of applications as an intermediate, i.e. in the production of allyl diglycol carbonate, 1-3 propanediol, poly (styrene –allyl alcohol), etc., which are used as plasticisers, crosslinking agents, and coating additives [4,6]. Several renewable sources can be envisaged as starting material for the synthesis of allyl alcohol whereby the most promising one – notably in terms of carbon economy – is glycerol. This molecule is the by-product formed during the transesterification of vegetable oils for the production of biodiesel [4]. Only a few systems for glycerol conversion to allyl alcohol with a cheap reductant have been reported [4,7], whereby the deoxydehydration reaction (DODH) is most promising. Fig. 1 displays the DODH of glycerol to allyl alcohol. This reaction requires a stoichiometric reductant (red), which is oxidized during the reaction (redO) [4].

A large diversity of catalytic systems for the DODH of glycerol in liquid phase have been reported in literature, including metal-free and transition metal-based catalysts. Notably the research of an optimal reductant and catalyst has become a subject of great interest, whereby H_2 or secondary alcohols in combination with rhenium-based catalysts were reported. First homogeneous catalytic systems were studied in 1996, by Cook *et al.* [8] using Cp^*ReO_3 for the DODH of diols into the corresponding olefin in the presence of PPh_3 as an oxo-acceptor (reductant). A yield in allyl alcohol of 67% at 125°C and 27h, was achieved. In 2012, Abu-Omar *et al.* [9] showed that $MeReO_3$ (MTO), a water and air tolerant homogeneous catalyst was able to transform glycerol under neat conditions in the presence of a base at 165°C, presenting a yield in the range of 75% of volatile products: allyl alcohol (1)/ acrolein(0.22)/ propanal(0.15), at full conversion. The result was correlated with the initial amount of glycerol, since glycerol was sacrificed as an internal reductant and eventually oxidized into dihydroxyacetone.

Instead of using glycerol as H-donor, various alcohols have been widely studied. Especially, the system of MTO and 3-octanol displayed an excellent yield of 90% at 170°C and 2.5h, as reported by Shiramizu

* Corresponding author.
E-mail address: benjamin.katryniok@ec-lille.fr (B. Katryniok).

https://doi.org/10.1016/j.mcat.2022.112856
Received 10 October 2022; Received in revised form 28 November 2022; Accepted 1 December 2022
Available online 7 December 2022

et al. [10] in 2012. They demonstrated that short-chain alcohols (less than 4 carbons) are ineffective H-donors. In contrast, for long chain alcohols ($\geq$ 5 C), secondary alcohols were found to be more favourable than primary alcohols. A year later, Boucher-Jacobs *et al.* [11] studied the use of ammonium perrhenate (APR) as catalyst because of its relatively low cost, greater hydrolytic stability, and solubility properties (easier recovery) in comparison to MTO. Despite the good performance of the secondary alcohol as reductant, such as 3-octanol (70% in yield), a primary alcohol (47% in yield) was preferred because of the formation of an aldehyde as co-product, which could be separated/recycled easier than the ketones resulting from the secondary alcohols. In 2014, Canale *et al.* [7] observed that catalysts such as Cp^*ReO_3, $Re_2(CO)_{10}$ were not active in DODH under neat and aerobic conditions, whereas MTO and rhenium trioxide (ReO_3) presented moderated performances (14% and 32%, respectively). A large number of solvents were tested under air and H_2 atmosphere such as 2,4-dimethyl-3-pentanol, 1-hexanol, 1,3 propanediol, 2-octanol and 1-phenyl-ethanol. Among this library of alcohols, 2,4-dimethyl-3-pentanol gave the best results with yields in allyl alcohol of 87% and 91% for MTO and ReO_3 under H_2 atmosphere, respectively.

Despite the high catalytic performance of these systems, their main drawback is the difficulty to recycle the catalyst [12]. Therefore, heterogeneous catalytic processes are of interest from the industrial point of view since they can be regenerated and reused for several catalytic cycles. Rhenium-based catalysts have been the main target of study: In 2016, Palkovits *et al.* [13] developed the first stable heterogeneous catalyst (ReO_x/TiO_2) for the DODH reaction. The corresponding catalyst showed a yield in allyl alcohol of 48-54%, using 3-octanol as reductant. Additionally, ReO_x/TiO_2 exhibited high stability with no deactivation over six runs and no traces of leaching. In the same year, Tomishige *et al.* [4] reported a higher yield (91%) in allyl alcohol using a ReO_x-Au/CeO_2 and even 93% with ReO_x-Ag/CeO_2 as a catalyst with hydrogen as reductant and 1,4-dioxane as solvent. In 2017, Kon *et al.* [14] studied other solid supports for the DODH of glycerol into allyl alcohol, working with alcohols as reductants and solvents. Impregnation of $HReO_4$ on SiO_2, TiO_2 and Al_2O_3 was carried out *via* incipient wetness impregnation method. Different kinds of alcohols such as 3-hexanol, 2-hexanol, 3-octanol, 2-butanol, 1-Hexanol, 1-octanol, 1-butanol, cyclohexanol, benzyl alcohol and 1-Phenylethanol were examined, whereby, long-chain secondary aliphatic alcohols gave highest yields in allyl alcohols (>84%).

Up to now, the influence of the support on the catalytic performance of heterogeneous Rhenium-based catalysts is still matter of debate. Notably ceria-based catalyst showed increased catalytic activity, which may be related to the intrinsic properties of the latter, such as surface oxygen vacancy concentration and the ratio of Ce^{3+}/ Ce^{4+}. In order to elucidate the role of ceria as support for ReO_x in the DODH reaction, a mesoporous ceria carrier was synthesized by the nano-casting method. The latter consists in depositing ceria on the surface of a stable matrix, such as silica and then remove the latter using NaOH or HF [15–17]. The as-obtained ceria supports were impregnated with rhenium oxide (ReO_x) and applied in the DODH reaction glycerol to allyl alcohol, using a secondary alcohol as a hydrogen donor and solvent.

2. Experimental methods

2.1. Synthesis

All commercial materials were used as received without further purification. A commercial mesoporous ceria support (HSA-5) was purchased from Solvay. A ceria-silica sample (CeO_2+SiO_2) was provided by Solvay (ECL9 #1503984). Perrhenic acid solution (75-80 wt.% $HReO_4$ in H_2O), glycerol (>99 wt.% of purity), allyl alcohol (98 wt.%), tetraethyl orthosilicate (TEOS,98%), Tetrapropylammonium hydroxide solution (20-25%TPAOH in H_2O), Cerium(III) nitrate hexahydrate ($Ce(NO_3)_3$*$6H_2O$, 99%), Activated Charcoal and solvents (99 wt.%) were obtained from Sigma Aldrich.

2.2. Support preparation

Hard template SBA-15: 20 g Pluronic P123 triblock copolymer ($EO_{20}PO_{70}EO_{20}$) were added to 250 g of distilled water. The mixture was stirred for 2h at room temperature. After that, 42.6 g of tetraethyl orthosilicate (TEOS, 98%, Aldrich), 142.8 g of concentrated HCl (35%) and 275g of distilled water were added and stirred for 1h at room temperature. The mixture was heated under stirring for 20h at 80°C. Finally, the white solids were recovered by filtration, washed with deionised water, and dried at 70°C during 24h in an oven. Thereafter, the products were calcined under static air at 550°C for 8h at a heating rate of 1°C/min.

Support CeO_2 using SBA-15 as hard template: For the synthesis of the mesoporous CeO_2, 2 g of SBA-15 were dispersed in 10 g of $Ce(NO_3)_3$*$6H_2O$ (99%, Aldrich) and dissolved in 40 mL of ethanol. The mixture was stirred at 60°C until solvent evaporation. Thereafter, the mixture was calcined to 450°C for 4h (1°C/min). After that, a second impregnation was carried out using 4.8 g of $Ce(NO_3)_3$*$6H_2O$ in 40 mL of ethanol. Following solvent evaporation at 60°C, the product was calcined in static air at 600°C for 4h (1°C/min). The siliceous template was later eliminated in 100 mL of a 2M NaOH solution at 25°C under stirring. The remaining material (mesoporous CeO_2) was centrifuged, washed with distilled water, and dried at 80°C.

Support CeO_2 using Activated Charcoal as hard template: 2 g of Activated charcoal were dispersed in 10 g of $Ce(NO_3)_3$*$6H_2O$ (99%, Aldrich) and dissolved in 40 mL of ethanol. The mixture was stirred at 25°C until solvent evaporation. Thereafter, the mixture was dried in static air at 200°C for 4h (1°C/min). After that, a second impregnation was carried out using 4.8 g of $Ce(NO_3)_3$*$6H_2O$ in 40 mL of ethanol. Following the solvent evaporation at 25°C, the product was dried in static air at 200°C for 4h (1°C/min) and then, calcined at 460°C for 2h (1°C/min) whereby the charcoal template was removed.

2.3. Catalyst preparation

Catalysts with different rhenium contents were prepared by an incipient-wetness impregnation method. Before each synthesis, 2 g of support was washed with distilled water and dried at 110°C (12h) and then calcined under static air at 500°C (3h). For the preparation of 10 wt % ReO_x catalyst, a diluted aqueous solution of $HReO_4$ was added to the support, which was obtained by diluting 400mg of the 75 wt.% $HReO_4$ aqueous solution with water (0.75 mL). The impregnated catalyst was dried at 110°C for 12 h and calcined under static air at 500°C for 3 h

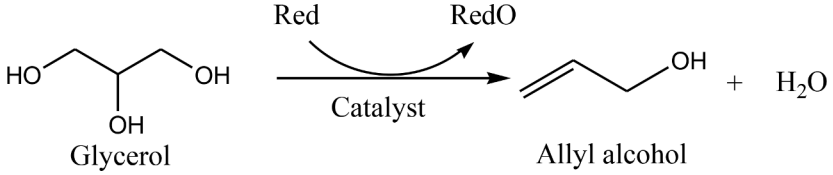

Fig. 1. General reaction pathway for the Deoxydehydration reaction. Red=reductant. RedO=oxidised reductant [4].

using a heating rate of 5°C/min. Concerning the preparation of 2.5 wt. %, 5 wt.% and 15 wt.% ReO_x supported catalysts, the synthesis proceeded as for 10 wt.% ReO_x but using 92, 190 and 635 mg of 75 wt.% $HReO_4$ aqueous solution, respectively.

2.4. Experimental procedure for DODH reaction of glycerol

The catalytic test for the DODH reactions were performed in a pressure resistant glass tubes equipped with a magnetic stirring bar charged with glycerol (92 mg, 1 mmol, purity in water >99%), 100 mg of catalyst, and 3.3 mL of solvent. The vessel was tightly sealed by a screw cap and the mixture was stirred (1300 rpm) in an oil bath maintained at 175 ℃ for 2.5 h. The inside temperature was evaluated exemplarily by introducing a thermocouple through the cap, showing a decay of 30°C. Correspondingly, we assume a reaction temperature of 145°C. After the reaction, the solution was cooled to room temperature and placed under ultrasonic irradiation for 5 min at 40°C of temperature to ensure a good homogeneity in a further analysis. The conversion and yield were determined by gas chromatography, using a GC instrument equipped with a CP-Wax52CB column (30m x 250 μm x 0.25 μm) and a flame ionization detector (FID).

2.5. Hot filtration test

The DODH reaction was carried out at 175°C, using 2-hexanol as solvent and 10%ReO_x/CeO_2+SiO_2 as catalyst. After 1 h of reaction, the catalyst was removed by filtration, using 0.45 μm filter paper. Then, the filtrate without the 10%ReOx/CeO_2+SiO_2 catalyst was heated again to 175°C (oil bath) for an additional 24h. The catalyst was recovered to further XRF analysis. For comparison, the identical procedure was used for a reaction time of 24h without catalyst removal.

2.6. Catalyst characterization

To determine the physical properties and chemical properties, the catalyst characterization was carried out using nitrogen adsorption/desorption, Transmission Electron Microscopy (TEM), X-ray Photoelectron Spectroscopy (XPS) and X-ray fluorescence (XRF) and X-ray diffraction (XRD).

2.6.1. Nitrogen adsorption/desorption

The surface areas, pore volumes and distributions of the pore sizes were determined by nitrogen adsorption/desorption at -190°C (liquid nitrogen) using a TriStar II Plus and a 3Flex apparatus from Micromeritics. Preliminary degassing of the samples was done at 75°C and 130°C for 90 min and 17.5h, respectively. The specific surface area (BET) was evaluated using the BET method (Brunauer, Emmet and Teller). In addition, the pore size distribution and the pore volume were calculated according to the Barrett-Joyner-Halenda (BJH) formula taking into account the data from desorption.

2.6.2. Transmission Electron Microscopy (TEM)

Selected catalysts were characterized by Transmission Electron Microscopy (TEM) to obtain local information at the nanometric and atomic levels on the morphology, structure, chemical composition, size and distribution of the nanoparticles on the support. The transmission electron microscope used was a FEI Tecnai G2 20 (TEM) equipped with an EDX (Energy-dispersive X-ray spectroscopy) micro-analysis, a Gatan energy filter (EELS), precession and electron tomography systems and an ORIUS CCD camera. This microscope uses a voltage of 200 kV for the acceleration of electrons. Sample preparation was done by inserting the support mesh into the catalytic converter to adhere the powder grains.

2.6.3. X-ray Photoelectron Spectroscopy (XPS)

XPS analyses were performed on a high-performance hemispheric analyzer VG Escalab 220 XL spectrometer and on a XPS KRATOS, AXIS UltraDLD with monochromatic Al Kα ($h\nu = 1486.6$ eV) radiation as the excitation source. The survey spectra (160 eV) and the high resolution spectra (20 eV) of the Re 4f, C 1s and O1s were collected. Binding energies were calibrated by setting the C 1s peak to 284.8 eV.

2.6.4. X-ray fluorescence (XRF)

X-ray fluorescence spectroscopy (XRF) was performed using an energy dispersive micro-X-Ray Fluorescence spectrometer M4 TORNADO (Bruker) with a Rhodium X-ray anode of 50 kV/600 mA enabling excitation of an area of 200 μm. The detector used was a Silicon-Drift-Detector Si(Li) with <145 eV resolution at 100000 cps (Mn Kα) and cooled with a Peltier cooling (-20°C). The measurement was done under vacuum (20 mbar). Quantitative analysis was done using fundamental parameter (FP) (standardless). To obtain accurate quantification of the components present in the catalysts, each sample was irradiated 35 times to obtain accurate mean values.

2.6.5. X-ray diffraction (XRD)

X-Ray Diffraction (XRD) was used to determine the crystal structure on a D8 Discover X-Ray Diffractometer from Bruker using a X-Ray tube in Cu (Kα) radiation (λ=1.54060 Å). The diffraction angle 2θ was in the 10-70° range with steps of 0.01° per second. The interpretation of the XRD patters was done from Diffract Eva software and the identification of the crystalline phase was done from reference standards.

2.6.6. Temperature-programmed reduction (TPR)

TPR analyses were performed on an automated AutoChem II 2920 Chemisorption Analyzer from Micromeritics. At first, 50 mg of catalyst were weighted and inserted into a glass reactor. Then, the sample was flushed with a mixture gas of 5 vol.% H_2 in Ar at room temperature. While the gas was flowing, the temperature of the sample was increased linearly at a ramp rate of 10°C/min up to 1000°C. The consumption of hydrogen by adsorption/reaction was monitored by a TCD detector to get quantitative information on the reducibility of the species present in the catalyst.

2.7. Theoretical modelling methods

Density functional theory (DFT) calculations were carried out using VASP software [18,19], with the Perdew-Burke-Ernzerhof (PBE) functional [20]. All the calculations were performed on a 5 × 5 × 1 k-mesh according to the Monkhorst−Pack scheme [21], with a cutoff energy of 400 eV in the plane augmented wave (PAW) framework [22]. We chose an electronic convergence criterion of 10^{-6} eV and an ionic convergence criterion of 0.05 eV/ Å. All those parameters allow to converge adsorption energies within ~0.05 eV. In order to assign oxidation sates we performed a Bader charge analysis, following the Henkelman method [23]. In agreement with previous studies [24–26], we considered the charge convergence criterion to be 0.10 e. That is, for any specific atom two successive oxidation states can be identified if their electronic charges are different by 0.10 e.

We started from the ReO_3 bulk structure reported in literature [27]. The optimized structure belongs to the cubic crystallographic system (Pm-3m space group) with a lattice parameter of 3.76 Å, in fair agreement with experiment [28]. Considering the (001) facet that has often been considered in computational studies for reason of its stability and reactivity [27–29], we focused on this surface in the following. We prepared a *p(2 × 2)* slab, with a thickness of three-metal oxide atomic layers from our DFT optimized bulk. We set a vacuum of 20 Å to prevent interaction between virtual periodic images in the *z* direction. Since the reaction proceeds in liquid medium, the external Re atoms are fully hydroxylated in our model. Also, in order to eliminate the dipolar moment inherent to metal oxide materials, we performed all our calculations on a symmetric slab along the *z* axis.

3. Results and discussion

3.1. Catalyst characterization of ceria-supported rhenium oxide catalyst

3.1.1. Textural characteristic and elemental composition

The textural characteristics of the samples are summarized in Table 1 For all the catalysts, the specific surface area and the pore volume were lower in comparison with the parent support. The latter can be explained by the filling of the pores of the support by the active phase, leading to a decrease of the overall pore volume. In the case of CeO_2+SiO_2 supported catalyst, the mean pore size of the catalysts was generally close to the one of the parent support.

The comparison of the textural properties of CeO_2+SiO_2 and CeO_2+SBA-15 supports (Table 1, entry 5 and 11, entry 13 and 15, respectively) before and after treatment with NaOH, showed an increased specific surface in case of CeO_2+SiO_2 after NaOH treatment (from 87.8 to 113.6 m^2g^{-1}) which was not observed in the case of CeO_2+SBA-15 (from 119.6 to 100.9 m^2g^{-1}). However, both showed an increased total pore volume after NaOH treatment (0.04 and 0.05 cm^3g^{-1}, respectively). The latter can be explained by the partial removing of the hard template from the corresponding support, as evidence by XRF (next paragraph). In the case of carbon as hard template (Table 1, entry 17 and 18), an increase in the textural properties was observed after calcination whereby the specific surface changed from 60.37 to 66.44 m^2g^{-1} and the total pore volume from 0.06 to 0.08 cm^3g^{-1}. In contrast, the textural properties of CeO_2 (HSA-5) (Table 1, entry 1 – 3) were not modified after NaOH treatment.

Concerning the isotherms, CeO_2 (HSA-5) and 10wt.% ReOx/ CeO_2 (HSA-5) showed type-IV isotherms, with the presence of a type H2 and H1 hysteresis loop, respectively (Fig. S2). The washing with NaOH does not show significant influence in the type of adsorption-desorption isotherm. Nevertheless, a strong change in the morphology was evidenced after Rhenium impregnation, since the supports present micro and mesoporous nature and the corresponding catalyst only mesoporous structure, most probably due to the blockage of the micropores by ReOx. Concerning CeO_2+SiO_2 as support, the corresponding catalysts presents similar adsorption-desorption isotherm (type IV) and mesoporous in nature (Fig. S3), both with the presence of a type H2 hysteresis. With the increase of the rhenium amount (2.5 wt.% to 15wt.%), the catalysts did not present any changes in their adsorption-desorption isotherm, only the decrease of the total pore volume with increasing amount of active phase was observed. According to fig. S4, after DODH reaction and NaOH washing, the isotherms of 10wt.% ReOx /CeO_2+SiO_2 remained unchanged (type IV). On the other hand, CeO_2+SBA-15 and 10wt.% ReOx/CeO_2+SBA-15 materials (Fig. S5), exhibited a change in the hysteresis loop from H2 to H1 (type IV isotherm) after washing with NaOH, indicating that the silica removal significantly affects the textural properties of the material. On the other hand, as seen from fig. S6, the presence of carbon on CeO_2 + carbon and 10wt.% ReOx/ CeO_2 + carbon do not affect the pore structure of the support, these materials present isotherm type III with H3 hysteresis loop, before and after calcination. Based on the above observations, it can be inferred that the washing with NaOH could change the porous structure of the support, whereas the calcination of the carbon template did not cause any modification.

The amounts of rhenium and silica in the synthesized catalyst and supports were determined by X-ray fluorescence (XRF) and are presented in Table 1. Concerning the amount of Re, one can see, that comparing the theoretical and actual loadings of the active phase, the latter were always lower. This might be due to the high volatility of rhenium oxide, mainly Re^{+7} species [30,31], resulting in some loss of Re during calcination. With respect to the hot filtration test, one can state that leaching of the active phase was not significant since the Re amount decreased only from 7.8 to 7.4 wt %.

In addition, according to the XRF analysis shown in Fig. S1, after the matrix removal procedure, no trace of sodium was identified on the surface of 10wt.% ReO_x/CeO_2+SiO_2 and 10wt.% ReOx/CeO_2+SBA-15. Comparing the silica content of these last catalysts (entry 8 and 12, entry 14 and 16, respectively), the removal of SBA-15 was higher than for the SiO_2 in the commercial catalyst (81% and 57%, respectively). However, this also evidenced that the hard template was not entirely removed.

3.1.2. X-ray diffraction and TEM

The X-ray diffraction (Figs. 2 and S7) showed for all catalysts only a ceria phase [32–35] with characteristic peaks close to the fluorite structure of CeO_2 (space group *Fm3m*; JCPDS 81-0792). The characteristic peaks corresponding to the (111), (200), (220), (311), (222), (400) crystal planes are located at $2\theta = 29.2°$, 33.1°, 47.5°, 57.6°, 59.0°, 69.4°, respectively. No rhenium oxide was detected by XRD, indicating either a good dispersion on the surface of the ceria support when using low amount of rhenium ($\leq$ 10wt.%) or the presence of an amorphous phase. However, characteristic peaks corresponding to Re_2O_7 crystals were detected on 15wt.% ReO_x/CeO_2+SiO_2, indicating a possible rhenium

Table 1
Textural properties of rhenium oxide-based catalysts.

Entry	Catalyst	Bet (m^2/g)	Mean pore size (Å)	Total pore volume (cm^3/g)	XRF element amount (%wt)			
					Re	Si	Ce	O
1	CeO_2 (HSA-5)	236.2	26.6	0.15				
2	10wt.% ReOx/ CeO_2 (HSA-5)	44.8	122.4	0.13	7.7	0.0	73.2	19.0
3	CeO_2 (HSA-5)[(b)]	236.6	27.2	0.16				
4	10wt.% ReOx/ CeO_2 (HSA-5)[(b)]	43.8	122.5	0.13	7.8	0.0	73.1	19.1
5	CeO_2+SiO_2	87.8	65.2	0.14	0.0	7.6	68.0	24.0
6	2.5wt.% ReOx/CeO_2+SiO_2	79.8	66.8	0.13	1.6	7.6	66	24.3
7	5wt.% ReOx/CeO_2+SiO_2	73.5	67.8	0.12	3.2	7.8	64.4	24.5
8	10wt.% ReOx/CeO_2+SiO_2	61.5	68.7	0.10	7.8	7.5	59.9	24.6
9	15wt.% ReOx/CeO_2+SiO_2	44.7	70.9	0.07	11.8	7.2	56.2	24.6
10	10wt.% ReO_x/CeO_2+SiO_2 [(a)]	25.4	96.8	0.06	7.4	7.8	60.2	24.2
11	CeO_2+SiO_2[(b)]	113.6	66.3	0.18				
12	10wt.% ReO_x/CeO_2+SiO_2[(b)]	75.8	80.5	0.15	8.4	3.3	66.5	21.6
13	CeO_2+SBA-15	119.6	56.5	0.16				
14	10wt.% ReOx/CeO_2+SBA-15	74.9	68.0	0.12	7.7	7.8	59.5	24.8
15	CeO_2+SBA-15[(b)]	100.9	87.2	0.21				
16	10wt.% ReOx/CeO_2+SBA-15[(b)]	51.2	121.7	0.15	7.8	1.5	70.4	20.2
17	CeO_2 + carbon	60.4	42.1	0.06				
18	CeO_2 + carbon [(c)]	66.4	51.1	0.08				
19	10wt.% ReO_x/ CeO_2 + carbon [(c)]	18.3	112.4	0.05	10.0	0.0	70.7	19.2

[(a)] Catalyst recovered after 3 cycles of reaction
[(b)] Washing with NaOH (2M), 3 times at 60°C
[(c)] Active carbon as hard template, carbon removal via calcination (air) at 500°C, 1h.

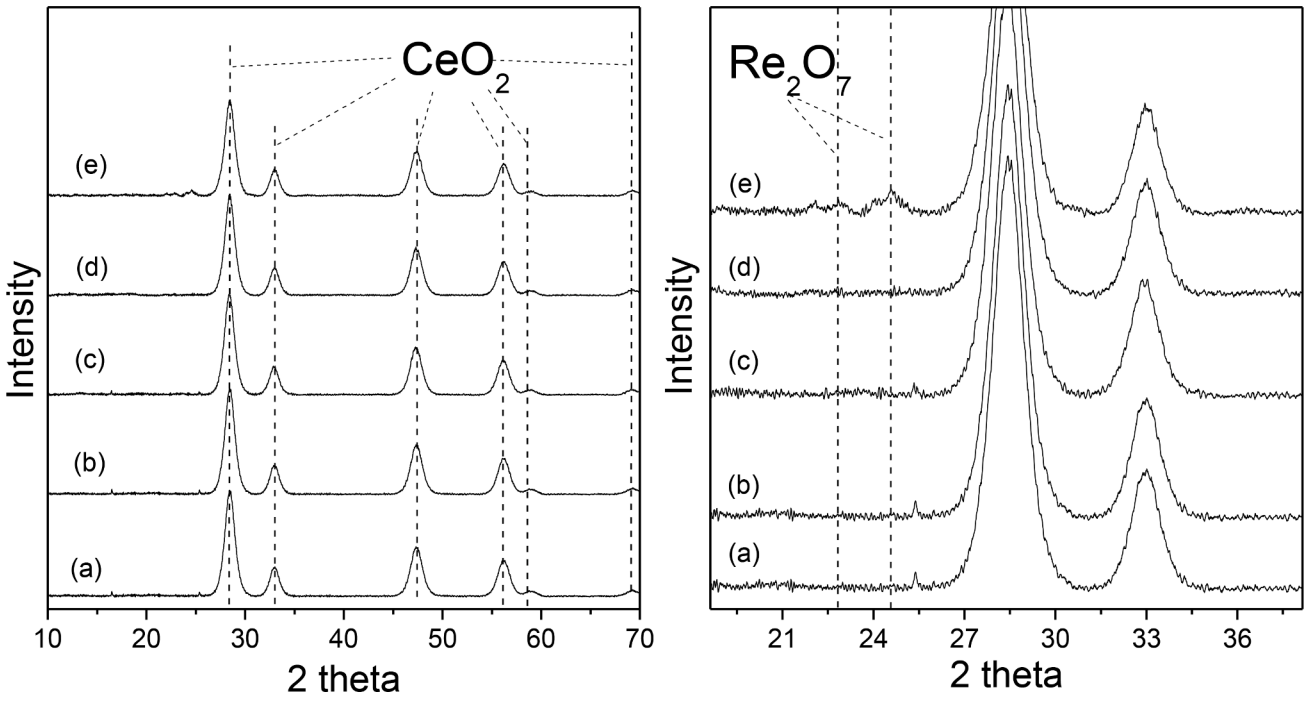

Fig. 2. XRD patterns for ReOx/CeO_2 catalyst (a) support CeO_2+SiO_2 (b) 2.5 wt.% ReOx/ CeO_2+SiO_2 (c) 5 wt.% ReOx/ CeO_2+SiO_2 (d) 10 wt.% ReOx/CeO_2+SiO_2 (e) 15 wt.% ReOx/CeO_2+SiO_2.

crystal growth [36–38], supporting the hypothesis of a good dispersion at low loading. These results were further confirmed by TEM evidencing the homogeneous dispersion of the active phase over the support by STEM-EDS elemental mapping images (Fig. 3). The image analysis also allowed to establish the particle size distribution, confirming the agglomeration of rhenium species in the case of 15wt.% as Re loading (Fig. 4) with a maximum particle size of 10 nm, contrary to 10wt.% Re, where the maximum particle size is around 3nm.

3.1.3. *Temperature-programmed reduction (TPR) analyses*

The temperature-programmed reduction (TPR) profiles of 10wt% ReOx/CeO_2 (HAS-5) and the bare CeO_2 (HAS-5) support are shown in

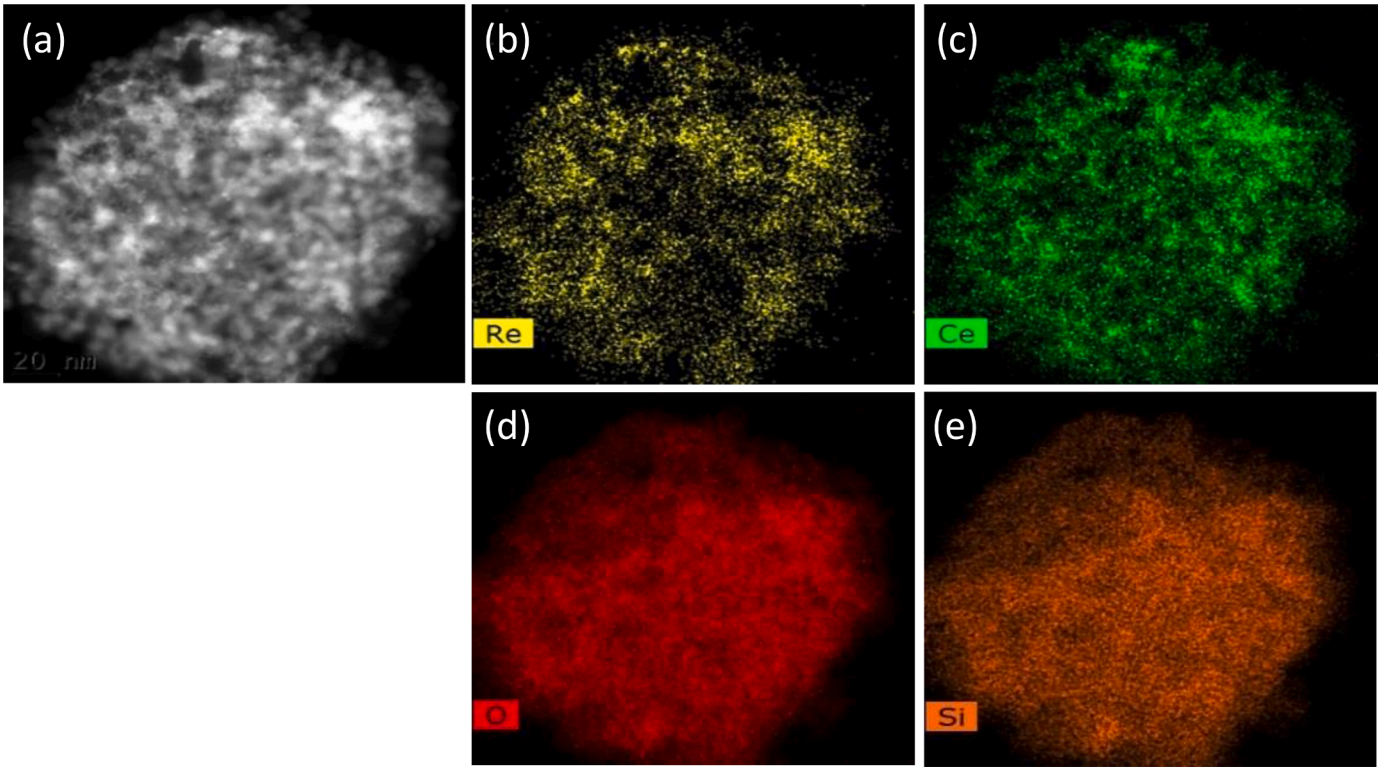

Fig. 3. HAADF-STEM and corresponding STEM-EDS elemental mapping images of 10wt.% ReOx/ CeO_2+SiO_2 (a) Representative HAADF-STEM image of precipitates, (b) (c) (d) (e) STEM-EDS maps for Re, Ce, O and Si, respectively.

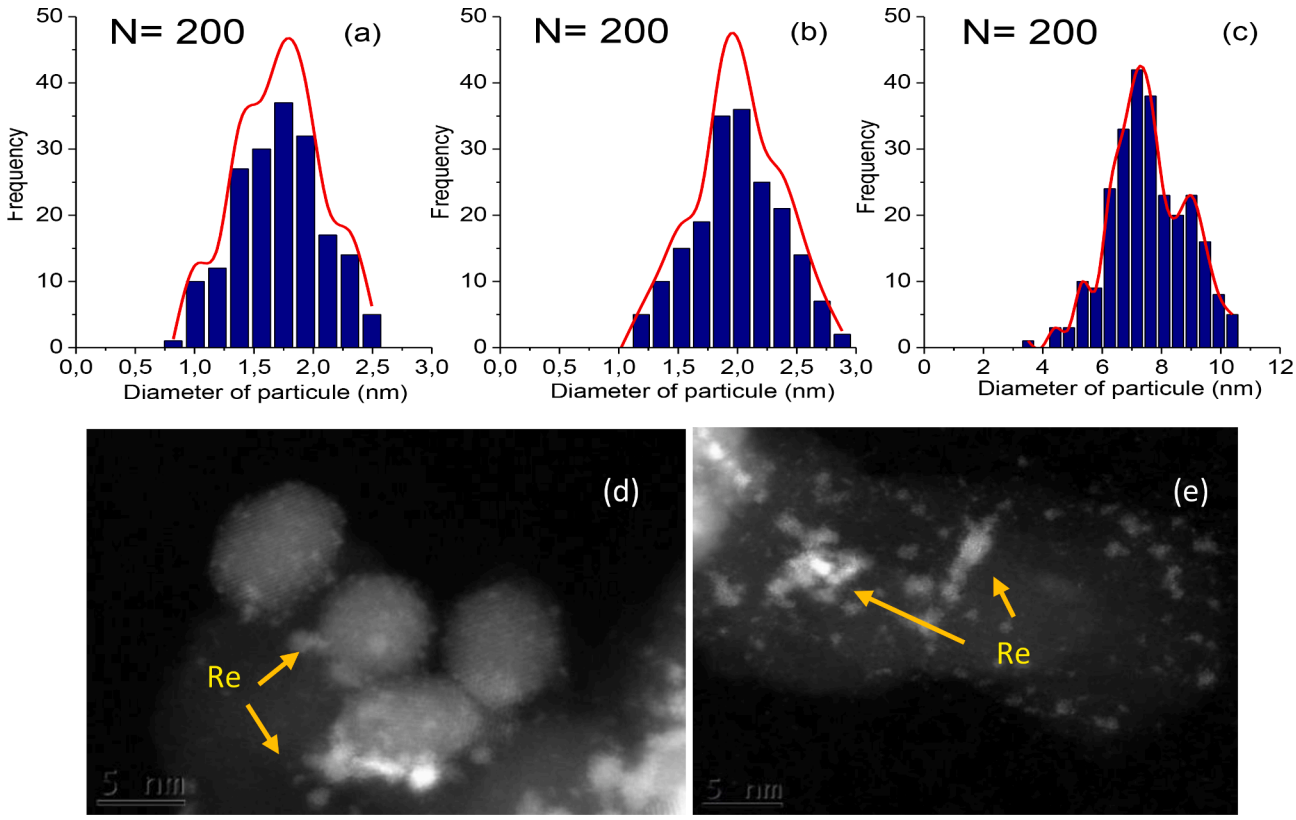

Fig. 4. Particle distribution of (a) 2.5wt.% ReOx/CeO_2 (b) 10 wt.% ReOx/CeO_2+SiO_2 (c)15wt.% ReOx/CeO_2+SiO_2 and DF-TEM image of (d) 10 wt.% ReOx/CeO_2+SiO_2 and (e) 15wt.% ReOx/CeO_2+SiO_2.

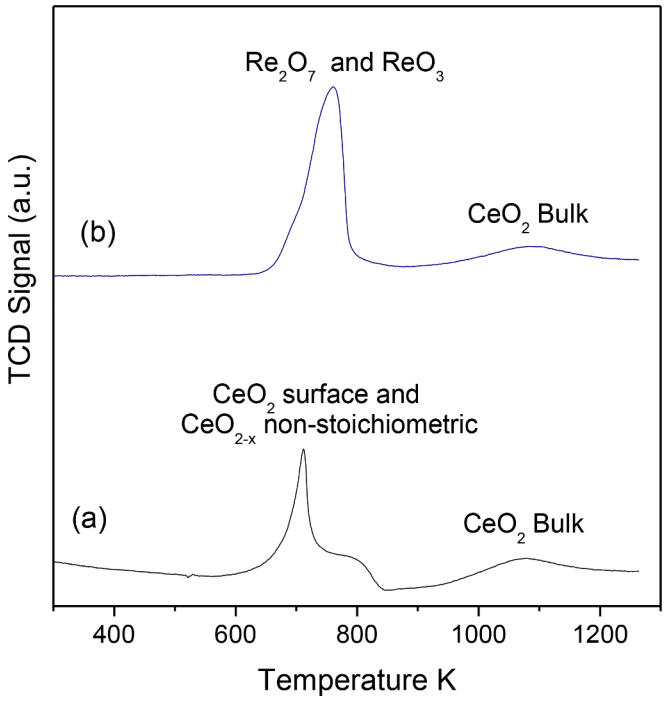

Fig. 5. TPR profiles of CeO_2-HAS-5 (a) and 10wt % ReOx/CeO_2-HAS-5 (b). Conditions: Sample (50 mg) and H_2/Ar (5%v/v, 50 cc/min) at heated rate of 10K/min.

Fig. 5. Both patterns have a broad signal above 900 K with almost constant area attributed to the oxygen species in bulk CeO_2. In the case of pure CeO_2 (a), the low temperature peak from 550 – 850K is related to the reduction of the most easily reducible surface-capping oxygen on CeO_2 [33,39,40]. Moreover, the overall consumption of hydrogen in the TPR of pure ceria is 1541 μmol/g, corresponding to an average Ce reduction of 53%. When 10 wt% of rhenium oxide is supported on ceria, the TPR pattern shows a sharp peak at 760 K [36] with a total H_2 consumption in the range of 600 – 850K of 1930 μmolH_2/g. This value was significantly larger (H_2/Re = 9.3) than for the total reduction of Re (H_2/Re = 3.5) suggesting that 20-25% of Ce were reduced simultaneously in this temperature range. In order to quantify the contribution of Ce and Re, it was tried to deconvolute the peak, but due to the bad fitting, no clear conclusion could be drawn.

3.1.4. X-ray Photoelectron Spectroscopy (XPS) Analyses

X-ray Photoelectron Spectroscopy (XPS) was performed to establish the change in oxidation states of the surface rhenium atoms during glycerol DODH reaction using 10 wt.% ReOx/CeO_2 (HSA-5) catalyst. The latter was deliberately chosen since no silica was present in this catalyst. Figure shows the Re *4f* and Ce*3d* spectra of the fresh and spent catalyst (1 cycle) and the curve fitted results. Concerning the fresh catalyst, the peaks with 46.3 and 45.1 eV binding energy (BE) were ascribed to Re $4f_{7/2}$ and correspond to Re^{7+} (84.09%) and Re^{6+} (15.91%), respectively [30,41–43]. In the case of the spent catalyst, the peaks shifted to lower BE. The peaks at 46.0, 44.7, 43.7, and 42.7 eV were assigned to Re^{7+}(39%), Re^{6+} (33%) and Re^{5+} (22.3%), Re^{4+}(5.65%), respectively. [30,41–43] These results are consistent with the formation of partially reduced ReO_X species during the reaction. Lupacchini *et al.* [44] evidence a reduction of rhenium during the DODH reaction using different Re species, namely Re^{7+} and $Re^{5+/4+}$ species, which was further confirmed by Tomishige *et al.* [45] for their ReO_x--Au/CeO_2 proposing a redox cycle with Re^{6+}/Re^{4+}. On the other hand, Jun Hee Jang *et al.* [41] found high catalytic activity of Re^{7+}/Re^{5+} species before and after reaction using Re nanoparticles and 3-octanol as reductant. In the present study, both Re^{5+} and Re^{4+} were found after

reaction, suggesting that both redox couples Re^{7+}/Re^{5+} and Re^{6+}/Re^{4+} are involved.

With respect to the differences in the studies (supported and non-supported Re), it seems possible that the support – namely ceria – prevent the deep reduction of rhenium ($<Re^{4+}$). In order to see if ceria was contributing as a redox couple in the DODH reaction, the Ce*3d* peaks of the fresh and spent catalyst were studied (Fig. 5). The peaks at 898.8, 890.16 and 882.9 eV BE were ascribed to Ce$3d_{5/2}$, corresponding to Ce^{4+} species and the peaks at 887.19 and 882.0 eV corresponded to Ce^{3+} species [46]. The fitting of the peaks showed that the Ce^{3+}/Ce^{4+} ratio before and after reaction was 0.28 and 0.27, respectively, meaning that no significant changes in the oxidation states took place during the reaction. In addition, with respect to results from literature, it is noteworthy that Ota *et al.* [4,36] observed a deep-reduction of rhenium until Re^0, under reaction conditions over ReOx−Pd/SiO_2 which they related to the deactivation of the catalyst. They also claimed a decrease of the catalytic activity in the DODH reaction using pre-reduced ReO_x−Pd/-CeO_2 catalyst without exposure to air in comparison with non-reduced catalyst, which was probably caused by the reduction of Ce^{4+} to Ce^{3+}. Since we employed NaOH treatment to eliminate the hard template, we analyzed the samples before and after treatment to see the influence of the template removal on the oxidation states of Ce and Re (Table 2, entries 2, 5 and 7). An increase in Re^{6+}/Re^{7+} and Ce^{3+}/Ce^{4+} ratio was observed in all catalysts. Considering that the reduction of Re is also involved in the catalytic cycle of DODH (Fig. 6 and Table 2, entry 3), whereas the reduction of ceria to Ce^{3+} was observed only after NaOH treatment but not from during the reaction, we can confirm the influence of the ceria on the catalytic performance and stability of DODH reaction which was further studied by DFT calculations.

3.2. Deoxydehydration (DODH) of glycerol

The influence of the preparation of CeO_2 using different hard templates on the catalytic performance was studied (Table 3) Similar yield in allyl alcohol was obtained using commercial CeO_2 (HSA-5), CeO_2+SiO_2 and CeO_2+SBA-15 as supports, with 84, 86 and 88%, respectively. The catalyst prepared using activated charcoal as hard template (Table 3, entry 7) showed a slightly lower yield in allyl alcohol of 80%. It is widely accepted that the use of high-surface-area supports increase the dispersion, stability and catalytic performance of ceria supported catalysts, [46–48]. Nevertheless, in the present study, the BET surface area and the type of silica matrix were not correlating to the yields (Table 3, entries 2, 8, 14, 19). Furthermore, the results also showed that the remaining silica had no effect on the catalytic performance in the DODH reaction. In contrast, when traditional removal of silica with NaOH (2M) was carried out in commercial CeO_2 (HSA-5), CeO_2+SiO_2 and CeO_2+SBA-15, a decrease in yield of around 14% was obtained (Table 3, entries 2, 4 and 6). As aforementioned, after the matrix removal procedure, no trace of sodium was identified on the surface of catalysts, therefore, the impact on the catalytic performance of DODH reaction was most probably related to the changes in the redox properties of the support, observed by the increase in Ce^{3+}/Ce^{4+} ratio.

The catalytic performance with different amounts of ReOx was studied using the CeO_2+SiO_2 support with 2.5 wt.%, 5 wt.%, 10 wt.% and 15 wt.%; the corresponding results and reaction conditions are shown in Table 4. The support does not show any catalytic activity toward allyl alcohol production (entry 1). Glycerol conversion increased as the amount of loaded rhenium oxide increased (entries 2-5). Since a good distribution of active phase was observed when 2.5, 5 and 10 wt.% amount of rhenium was used (entries 2-4), since similar selectivity was achieved (around 85%), and complete conversion with two of them (5 and 10 wt %); 2.5 wt.% shows still fair activity with a conversion of 90% (entry 2). When 15 wt.% of rhenium was used, a decreased selectivity of 81% was observed, which could be explained by the clustering of rhenium as observed by XRD (entry 5). Considering that 10 wt.% ReOx / CeO_2+SiO_2 was the catalysts giving highest yield (86%), this catalyst was used in the following tests for optimizing the reaction conditions and the recyclability. The influence of the glycerol amount and the reaction time are reported in fig. S8: increasing the glycerol concentration to more than 5wt.% at a constant glycerol/catalyst ratio, affect negatively the reaction yield, possibly due to mass transfer limitations caused by the high viscosity of glycerol. Regarding the reaction kinetics (Fig. S9), the selectivity is optimal for a time of 2.5h. For a longer reaction time, secondary reaction pathways take place, leading to the degradation of allyl alcohol. The detection of other molecules via GC/MS during the DODH reaction was limited (Fig. S10), and therefore further investigation is required to understand the reaction pathways involved in the degradation.

Regarding the possible scale-up to a continuous process, the catalytic recyclability of 10 wt.% ReO_x/ CeO_2+SiO_2 was studied. The DODH of glycerol was carried out at 175°C, 1300 rpm and 2h as the reaction conditions. Between each cycle, the catalyst was only washed with the reaction solvent (2-hexanol), to avoid glycerol and allyl alcohol accumulation. The relative amount of glycerol to the quantity of recovered catalyst from the previous run was kept constant. The corresponding catalyst did not lose any activity with reuse: the yield remains stable at around 58% after three cycles (Fig. 7). This result also indicates that the active catalyst was not a homogeneous rhenium complex resulting from the dissolution of the rhenium oxide supported on ceria. This was subsequently validated by a hot filtration test, where the catalyst was filtered after 1h of reaction, and the filtrate showed no further increase in yield of allyl alcohol after 24h of reaction (Fig. 8), which was also underlined by the absence of Re leaching evidenced by XRF (Fig.S1).

The influence of the sacrificial alcohol was studied for the 10 wt.% ReO_x/ CeO_2+SiO_2 catalyst. The results are reported in Table 5. High yields in allyl alcohol were observed using long-chain aliphatic secondary alcohols, such as 2-hexanol, 4-methyl-2-pentanol (MIBC), 3-octanol and 2-pentanol (86%, 85%, 79%, and 65%, respectively) (Table 5, entries 1-4). In contrast, the performance of primary alcohols such as 1-heptanol (Table 5, entry 5) and short-chain aliphatic secondary alcohols, such as 2-butanol (Table 5, Entry 6), gave a yield in allyl alcohol of 22% and 24%, respectively. Cyclic alcohol (cyclohexanol)

Table 2
Summary of XPS data of ReOx/CeO_2-HAS-5, ReOx/CeO_2+SiO_2 and ReOx/CeO_2+SBA-15, before and after NAOH TREATMENT.

Entry	Catalyst	Binding energy /eV									Molar ratio	
		Re 4f $_{7/2}$				Ce 3d $_{5/2}$						
		Re^{VII}	Re^{VI}	Re^{V}	Re^{IV}	Ce^{IV}			Ce^{III}		Re^{VI}/Re^{VII}	Ce^{III}/Ce^{IV}
1	10wt.%ReOx/CeO_2-HSA-5	46.3	45.1	-	-	898.7	889.9	882.9	887.2	882.4	0.19	0.28
2	10wt.%ReOx/CeO_2-HSA-5 [(a)]	46.1	44.6	-	-	989.4	888.2	882.7	884.5	882.4	0.24	0.62
3	10wt.%ReOx/CeO_2-HSA-5 [(b)]	46.0	44.7	43.7	42.7	898.3	889.3	882.3	885.3	882.2	0.85	0.27
4	10wt.%ReOx/CeO_2+SiO_2	46.7	45.07	-	-	898.7	888.7	882.8	884.5	881.7	0.32	0.33
5	10wt.%ReOx/CeO_2+SiO_2 [(a)]	46.4	45.3	-	-	898.7	888.6	882.6	884.3	881.1	0.90	0.53
6	10wt.%ReOx/CeO_2+ SBA-15	46.4	46.6	-	-	898.5	888.5	882.5	884.0	881.3	1.09	0.40
7	10wt.%ReOx/CeO_2+ SBA-15 [(a)]	46.2	45.3	-	-	898.4	888.29	882.7	884.3	881.3	1.31	0.67

[(a)] Fresh catalyst, After NaOH treatment
[(b)] Used catalyst, Without NaOH treatment

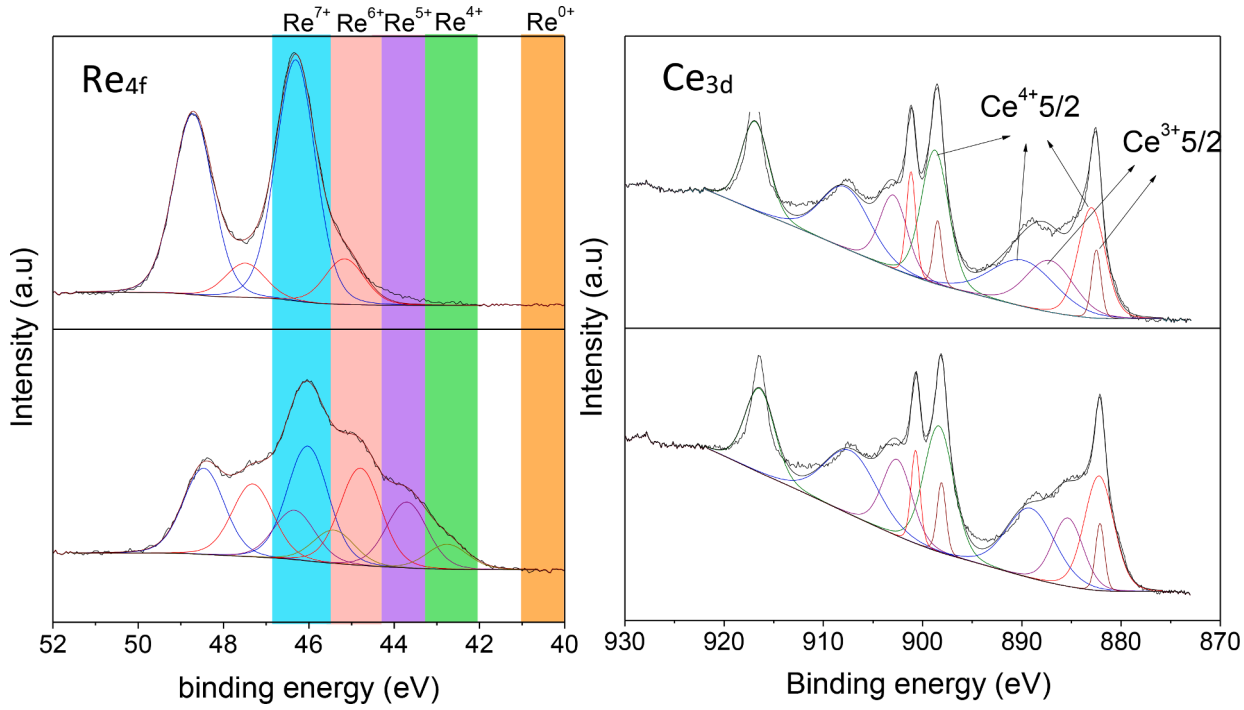

Fig. 6. . XPS spectra of the 10%ReOx/CeO_2 -HSA-5 catalyst before (up) and after reaction (down) in Re 4f and Ce 3d regions. The binding energy zone of Re4f7/2 for the different oxidation states are indicated in the colored regions. Reference: C 1s = 284.6 eV. Normalized by area of Ce 3d XPS.

Table 3
Influence of ceria synthesis in the performance of DODH of glycerol[(a)].

Entry	Catalyst	Conversion (%)[(b)]	Yield (%)[(b)]
1	10wt.% ReOx/ CeO_2 (HSA-5)	>99	84
2	10wt.% ReOx/ CeO_2 (HSA-5)[(c)]	95	77
3	10wt.% ReOx/CeO_2+SiO_2	>99	86
4	10wt.% ReOx/CeO_2+SiO_2[(c)]	93	72
5	10wt.% ReOx/CeO_2+SBA-15	>99	88
6	10wt.% ReOx/CeO_2+SBA-15[(c)]	91	73
7	10wt.% ReOx/ CeO_2 + carbon [(d)]	95	80

[(a)] Reaction conditions: Glycerol (1.0 mmol), Catalyst (100 mg), 2-Hexanol (3.33 mL), 175°C (oil bath), 1300 rpm, 2.5 h
[(b)] Conversion and yield based on glycerol, determined by GC analysis with benzene as an internal standard.
[(c)] Washing with NaOH (2M), 3 times at 60°C
[(d)] Active carbon as hard template. Carbon removal via calcination (air) at 500°C, 1h

Table 4
Performances of the ReO_x/CeO_2+SiO_2 catalysts in the DODH reaction of glycerol to allyl alcohol [(a)].

Entry	Catalyst	Conversion (%)[(b)]	Yield (%)[(b)]
1	CeO_2+SiO_2	3	0
2	2.5wt.% ReOx/CeO_2+SiO_2	91	77
3	5wt.% ReOx/CeO_2+SiO_2	>99	84
4	10wt.% ReOx/CeO_2+SiO_2	>99	86
5	15wt.% ReOx/CeO_2+SiO_2	>99	81

[(a)] Reaction conditions: Glycerol (1.0 mmol), Catalyst (100 mg), 2-hexanol (3.3 mL), 175°C (oil bath), 1300 rpm, 2,5 h
[(b)] Conversion and yield based on glycerol, determined by GC analysis with benzene as an internal standard.

showed a moderated yield of 21%. In general, in accordance with the literature, aliphatic secondary alcohols having longer chains are more suitable H-donors for DODH of glycerol.[1,11,41]

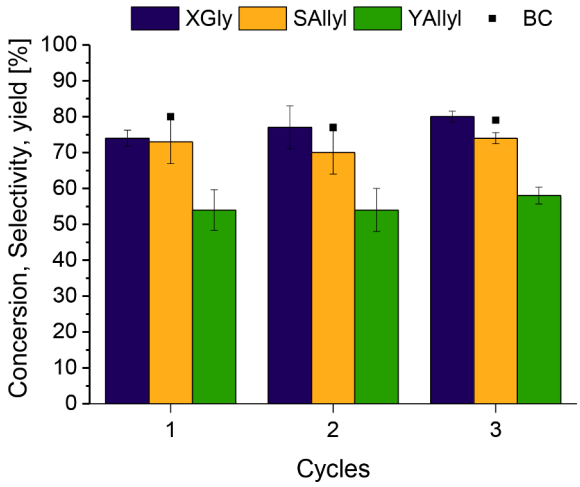

Fig. 7. Recyclability test. Reaction conditions: Glycerol (1.0 mmol), 10%ReOx/CeO_2+SiO_2 (100 mg), 175°C (oil bath), 2h, 2-hexanol (3.3 mL), 1300 rpm. The relative amount of glycerol to the quantity of recovered catalyst from each run was kept constant. X_{gly} = conversion of glycerol, S_{Allyl} = Allyl alcohol Selectivity, Y_{allyl} = Allyl alcohol performance and BC = Carbon Balance.

3.3. Proposed Reaction mechanism

As previously indicated, the redox properties and the ceria support play a vital role in the catalytic activity of DODH of glycerol. The reaction mechanism proposed in this study is summarized in Fig. 9. Reduced ceria surface consists of a mixture of Ce^{3+} and Ce^{4+} and numerous O-vacancies since Re centers act as the electron acceptor, leading to the formation of oxygen vacancies at the interfacial sites of Re and CeO_2 [49] and the eventual stabilization of rhenium seven species, due to strong metal support interactions at Ce^{3+} sites [50].

In general, the proposal reaction mechanism consists in five elementary reaction steps. (1) Represents the dissociative adsorption of

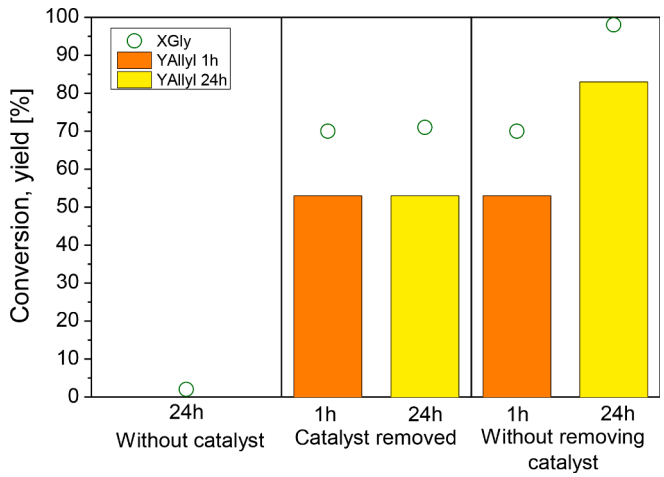

Fig. 8. Hot filtration test. (a) 10%ReOx/CeO_2+SiO_2 undergo glycerol DODH with 2-hexanol in pressure glass reactor for 1h at 170°C. Catalyst was removed by filtration at high temperature, and the filtrate without 10%ReOx/CeO_2+SiO_2 was heated to 175°C (oil bath) for an additional 24h. (b) Glycerol conversion and yield of allyl alcohol for 24h without removing catalyst were recovered at 1h and 24h for comparison test. (c) Glycerol conversion without catalyst was studied for another comparison test.

Table 5
Effect of solvent on the performances in DODH reaction of glycerol to allyl alcohol [(a)].

Entry	Solvent	Conversion (%)[(b)]	Yield (%)[(b)]
1	2-Hexanol	>99	86
2	4-Methyl-2-pentanol	>99	85
3	3-Octanol	>99	80
4	2-Pentanol	82	65
5	1-Heptanol	45	22
6	2-Butanol	37	24
7	Cyclohexanol	35	21

[(a)] Reaction conditions: Glycerol (1.0 mmol), 10wt.% ReOx/ CeO_2+SiO_2 (100 mg), Solvent (3.3 mL), 175°C (oil bath), 1300 rpm, 2.5 h
[(b)] Conversion and yield based on glycerol, determined by GC analysis with benzene as an internal standard.

the sacrificial alcohol on the reduced ceria. According to the literature, the adsorption of secondary alcohols occurs at O-coordination vacancies, on the under coordinated Ce^{4+} cations - Lewis acid sites - located in the second layer beneath the O-terminated ceria, where the remaining alkoxy is stabilized [51,52]. Considering that the alkoxy is adsorbed on the Lewis acid site next to the rhenium site (VII), desorption step leads the formation of the corresponding ketone via dehydrogenation reaction (2). In agreement with the studies of Abu-Omar *et al.* [53] et Palkovits *et al.* [13], rhenium particles catalyse the dehydrogenation of alcohols. In this study, the corresponding ketone (2-hexanone) was detected via GC as secondary product in the case of 2-hexanol as H-donor (Fig. S10). Regarding the results obtained in Table 5, the changes in catalyst activity for the different alcohols indicates that dehydrogenation reaction is the rate limiting step in the coupling system [49,50]. The H atom is transferred to the rhenium site (VII) surface via spill over mechanism on the ceria surface [54], allowing the reduction of Re (3). Then the condensation of glycerol take place on the reduced rhenium (V) site followed by the extrusion of allyl alcohol along with the oxidation of rhenium site (from V to VII), closing the redox cycle of rhenium [50,55,9].

3.4. DODH reaction mechanism simulation

To explain the presence of the alternative redox cycle including the Re^{4+}/Re^{6+} couple, DFT calculations were performed. Considering the determining role of O/OH vacancy for the reactivity of metal oxide/hydroxide surfaces [26,56] we modelled the glycerol DODH to allyl alcohol reaction both at the perfect and the OH vacant ReO_xH_y surfaces. First, regarding the reaction at the perfect surface (see Fig. 10), the catalytic cycle starts with the adsorption of glycerol on the surface. Due to its multiple hydroxide groups and its high flexibility, glycerol molecule can adopt a huge range of conformations. Following previous studies from Sautet and co-workers [57,58],we focused here on the most stable gas conformation with the two terminal hydroxide groups engaged in a mutual H bond. On the Re (hydr-)oxide surface, the most stable glycerol configuration is obtained when it adsorbs via the two terminal OH-groups. The structure is stabilized by H-bonds between the molecule and the hydroxylated surface, resulting in an adsorption energy of -0.6 eV (Fig. 10, left, Int2). In the following step, glycerol becomes dehydrated on the terminal C-atom forming a C-O-Re bridge (Fig. 10, left, Int3). The corresponding step is slightly endothermic with a +0.37 eV. Then, the as-formed intermediate is hydrogenated liberating allyl alcohol and water, leaving behind a partially oxidized ReO_xH_{y-2} surface (Fig. 10, left, Int4), which becomes finally regenerated by hydrogen from the sacrificial alcohol (Fig. 10, left, Int1). From the reaction energies, one can see that the determining step is the first dehydration leading to the C-O-Re bridge (Int2 to Int3), which is endothermic, compared to all other steps. In order to access the oxidation states of Re during the catalytic cycle, the Bader charge was calculated (Fig. 10, right). From these figures, on cane distinguish three successive electronic charge levels, 2.5, 2.6 and 2.7 e, respectively corresponding to Re^{5+}, Re^{6+}, Re^{7+}. Correspondingly, this first model, only explains the redox couple Re^{5+}/Re^{7+}.

Then, the reaction at the OH defected surface was simulated, that is with one exposed bare Re atom. As it can be observed on Fig. 11, the catalytic steps are globally identical to our previous calculations for the non-vacant surface, with only two major differences. Whereas the formation of the C-O-Re bridge (Int2 to Int3) on the non-vacant surface is endothermal, the latter is exothermal for the vacant surface (-0.62eV vs. +0.37eV). On the other hand, whereas the hydrogenation step for the non-vacant surface is exothermal or non-thermal (-0.12eV), the latter is endothermal for the vacant surface (+0.64eV). Finally, the Bader charges were calculated (Fig. 11, right) showing significant differences in the present oxidation states with at least four states, attributed to Re^{7+}, Re^{6+}, Re^{5+} and Re^{4+}. These results are thus in agreement with the experimentally observed redox couples Re^{5+}/Re^{7+} and Re^{4+}/Re^{6+}.

As we mentioned above, vacancy formation is determining for metal oxide reactivity. Hence, it is reasonable to consider that some vacancies are present in the system. In addition, it is worth mentioning that the cost of OH vacancy formation of the vacancy corresponds to an energy barrier of +1.13 eV, which is acceptable. Therefore, it is highly probable that some defected Re sites are effectively present on the ReO_xH_y surfaces. Also, there is no clear evidence in our calculations that one mechanism is more likely to happen than the other. That is why, both pathways should be considered as potentially proceeding in a simultaneous way at different surface sites.

4. Conclusion

The Deoxydehydration (DODH) of glycerol to allyl alcohol was studied over ceria-supported rhenium oxide catalyst. SiO_2 and carbon were used as hard templates in the synthesis of mesoporous ceria materials, via nanocasting method. Upon NaOH treatment, the removal of the hard template was only partial, but caused a decreased catalytic performance. Thus, best performance was observed for non-treated ceria-supported rhenium oxide catalysts (10 wt.% ReO_x/ CeO_2+SiO_2) yielding up to 86% allyl alcohol, using 2-hexanol and 4-methyl-2-pentanol as a H-donor and solvent. The corresponding catalyst was reusable for 3 cycles without reactivation step. Furthermore, no evidence of leaching was observed via hot filtration test, which encourages us to

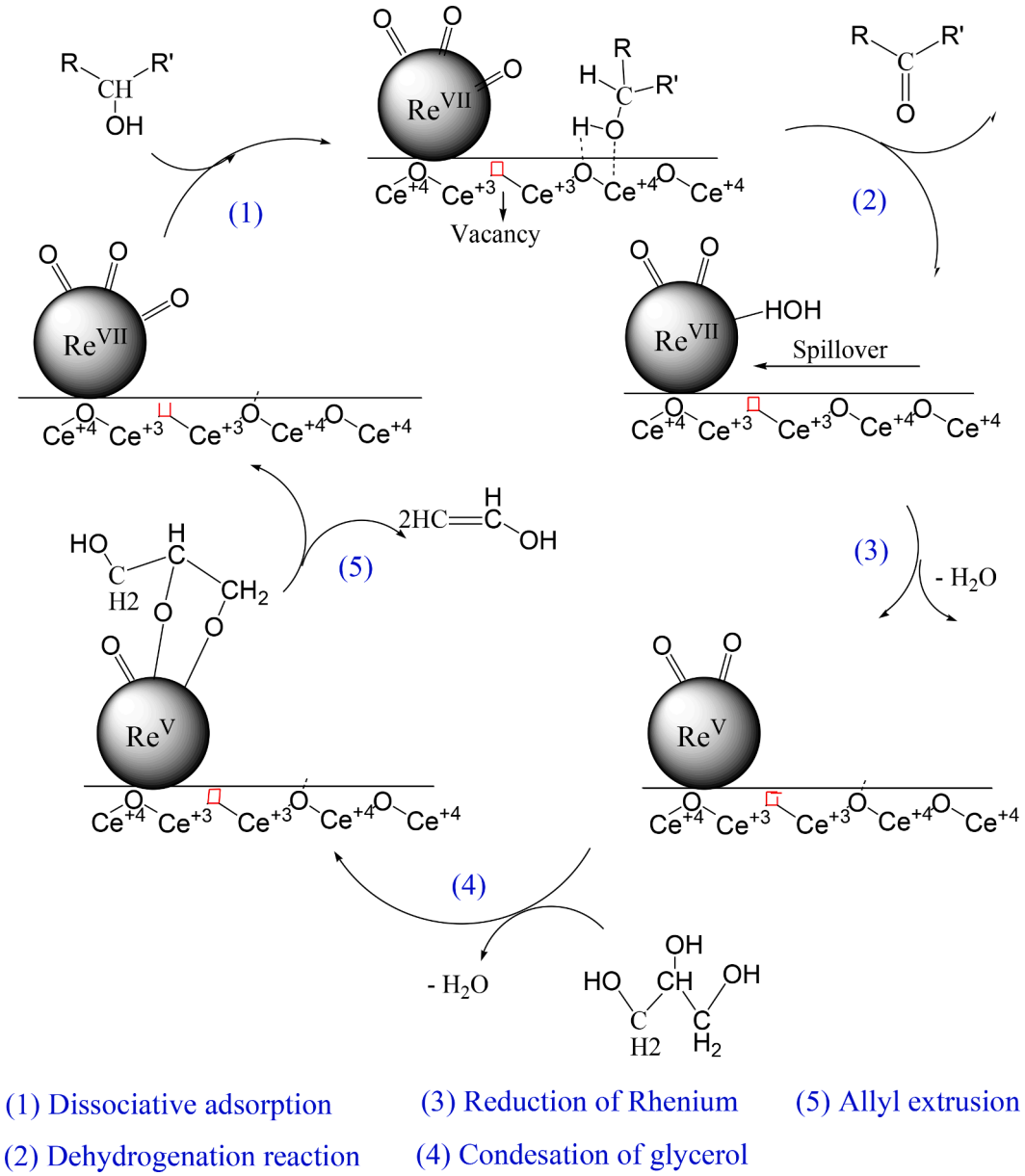

Fig. 9. Proposed reaction mechanism of DODH of glycerol into allyl alcohol catalysed by ceria-supported rhenium oxide using secondary alcohols as hydrogen donors.

study the catalytic performance in a continuous reactor and to perform a process simulation (i.e. with ASPEN) in the near future.

The results of the nitrogen physisorption showed no correlation between the surface are and catalytic activity even though good dispersion of the active phase was evidenced by X-ray diffraction and TEM when using low amount of rhenium ($\leq$ 10wt.%), suggesting that the catalytic performance is mainly governed by the redox properties. Since TPR results suggested that Ce could play a role in the reduction of rhenium species, a XPS study was performed showing that the Ce^{3+}/Ce^{4+} ratio was not affected by the DODH reaction but significantly changed upon NaOH treatment of the support. Additionally, this study showed that the two redox couples Re^{7+}/Re^{5+} and Re^{6+}/Re^{4+} are involved during DODH of glycerol to allyl alcohol, which made us proposing a reaction mechanism based on the presence of Ce^{3+} and Ce^{4+} sites and numerous O-vacancies. The latter was further validated by DFT calculations confirming the presence of the redox couples Re^{5+}/Re^{7+} and Re^{4+}/Re^{6+} in the case of a O-defect ReO_xH_y surface.

CRediT authorship contribution statement

Karen Silva Vargas: Investigation, Formal analysis, Visualization, Writing – original draft. **Jeremie Zaffran:** Conceptualization, Investigation, Data curation, Writing – original draft, Visualization. **Marcia Araque:** Conceptualization, Supervision, Writing – review & editing. **Masahiro Sadakane:** Conceptualization, Supervision, Funding acquisition. **Benjamin Katryniok:** Funding acquisition, Supervision, Writing – original draft, Writing – review & editing.

Declaration of Competing Interest

The authors declare that they have no known competing financial interests or personal relationships that could have appeared to influence the work reported in this paper.

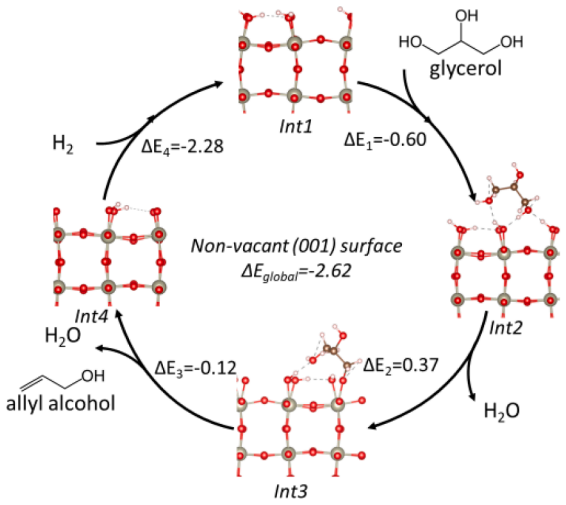

Non vacant surface				
Eff. Charge (e)	Int1	Int2	Int3	Int4
External atoms Re1	2.5	2.5	2.5	2.6
Re2	2.6	2.5	2.5	2.6
Re3	2.5	2.6	2.5	2.7
Re4	2.6	2.5	2.5	2.7
Re5	2.5	2.5	2.5	2.6
Re6	2.5	2.5	2.5	2.6
Re7	2.5	2.5	2.5	2.6
Re8	2.6	2.5	2.6	2.6
External atoms Re9	2.5	2.5	2.5	2.6
Re10	2.6	2.5	2.6	2.5
Re11	2.5	2.6	2.6	2.7
Re12	2.6	2.6	2.7	2.6

Fig. 10. DODH of glycerol reaction pathway on fully hydroxylated ReO_3 (001) surface (left); Effective charges (Eff. Charge) obtained from Bader analysis (right). Energies are given in eV, and effective charges in multiple of the elementary charge, e. Balls and sticks color code: grey, Re; red, O; pinkish, H. For the right table, the blue Re denotes the most external atoms, exposed to glycerol substrate. The various colors in the table represent the three electronic charge levels.

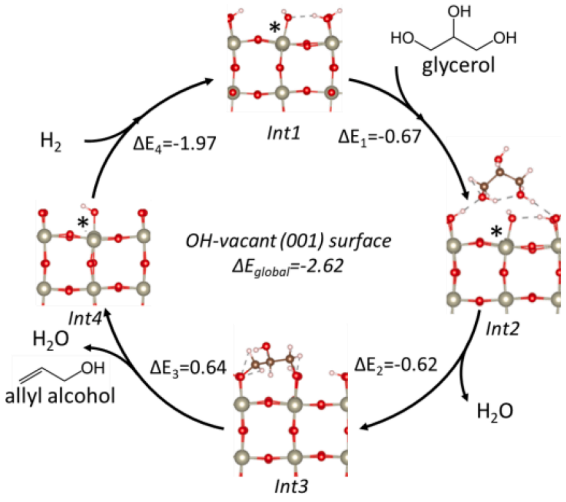

OH vacant surface				
Eff. Charge (e)	Int1	Int2	Int3	Int4
External atoms Re1	2.5	2.5	2.5	2.5
Re2	2.6	2.5	2.6	2.7
Re3	2.4	2.4	2.6	2.5
Re4	2.6	2.4	2.4	2.5
Re5	2.5	2.5	2.5	2.5
Re6	2.5	2.5	2.6	2.7
Re7	2.5	2.6	2.6	2.4
Re8	2.5	2.6	2.6	2.5
External atoms Re9	2.5	2.5	2.5	2.5
Re10	2.6	2.5	2.6	2.5
Re11	2.3	2.4	2.5	2.5
Re12	2.5	2.5	2.6	2.6

Fig. 11. DODH of glycerol reaction pathway on vacant ReO_3 (001) surface (left); Bader charges (right). Effective charges (Eff. Charge) obtained from Bader analysis (right). Energies are given in eV, and effective charges in multiple of the elementary charge, e. Balls and sticks color code: grey, Re; red, O; pinkish, H. For the right table, the blue Re denotes the most external atoms, exposed to glycerol substrate. The various colors in the table represent the three electronic charge levels.

Data availability

Data will be made available on request.

Supplementary materials

Supplementary material associated with this article can be found, in the online version, at doi:10.1016/j.mcat.2022.112856.

References

[1] J. Gossett, R. Srivastava, Rhenium-catalyzed deoxydehydration of renewable biomass using sacrificial alcohol as reductant, Tetrahedron Lett. 58 (39) (2017) 3760–3763.
[2] A.J. Ragauskas, C. Williams, B. Davison, G. Britovsek, J. Cairney, C. Eckert, W. Frederick, J. Hallett, D. Leak, C. Liotta, J. Mielenz, R. Murphy, R. Templer, T. Tschaplinski, The path forward for biofuels and biomaterials, Science 311 (5760) (2006) 484–489.
[3] J. Tendam, U. Hanefeld, Renewable chemicals: Dehydroxylation of glycerol and polyols, ChemSusChem 4 (8) (2011) 1017–1034.
[4] S. Tazawa, N. Ota, M. Tamura, Y. Nakagawa, K. Okumura, K. Tomishige, Deoxydehydration with molecular hydrogen over ceria-supported rhenium catalyst with gold promoter, ACS Catal 6 (10) (2016) 6393–6397.
[5] A. Jefferson, R.S. Srivastava, Re-catalyzed deoxydehydration of polyols to olefins using indoline reductants, Polyhedron 160 (2019) 268–271.
[6] G. Sánchez, B.Z. Dlugogorski, E.M. Kennedy, M. Stockenhuber, Zeolite-supported iron catalysts for allyl alcohol synthesis from glycerol, Appl. Catal. A Gen. 509 (2016) 130–142.
[7] V. Canale, L. Tonucci, M. Bressan, N. D'Alessandro, Deoxydehydration of glycerol to allyl alcohol catalyzed by rhenium derivatives, Catal. Sci. Technol. 4 (10) (2014) 3697–3704.
[8] G.K. Cook, M.A. Andrews, Toward nonoxidative routes to oxygenated organics: STEREOSPECIFIC deoxydehydration of diols and polyols to alkenes and allylic alcohols catalyzed by the metal oxo complex (C5Me5)ReO_3, J. Am. Chem. Soc. 118 (39) (1996) 9448–9449.
[9] J. Yi, S. Liu, M.M. Abu-Omar, Rhenium-catalyzed transfer hydrogenation and deoxygenation of biomass-derived polyols to small and useful organics, ChemSusChem 5 (8) (2012) 1401–1404.
[10] M. Shiramizu, F.D. Toste, Deoxygenation of biomass-derived feedstocks: oxorhenium-catalyzed deoxydehydration of sugars and sugar alcohols, *Angew. Chemie - Int. Ed.* 51 (32) (2012) 8082–8086.
[11] C. Boucher-Jacobs, K.M. Nicholas, Catalytic deoxydehydration of glycols with alcohol reductants, ChemSusChem 6 (4) (2013) 597–599.
[12] D.J. Cole-Hamilton, Homogeneous catalysis - New approaches to catalyst separation, recovery, and recycling, Science 299 (5613) (2003) 1702–1706.

[13] L. Sandbrink, E. Klindtworth, H.U. Islam, A.M. Beale, R. Palkovits, ReO_x/TiO_2: a recyclable solid catalyst for Deoxydehydration, ACS Catal 6 (2) (2016) 677–680.

[14] Y. Kon, M. Araque, T. Nakashima, S. Paul, F. Dumeignil, B. Katryniok, Direct conversion of glycerol to allyl alcohol over alumina-supported rhenium oxide, ChemistrySelect 2 (30) (2017) 9864–9868.

[15] W. Shen, X. Dong, Y. Zhu, H. Chen, J. Shi, Mesoporous CeO_2 and CuO-loaded mesoporous CeO2: Synthesis, characterization, and CO catalytic oxidation property, Microporous Mesoporous Mater. 85 (1–2) (2005) 157–162.

[16] S. Jun, J.Sang Hoon, R. Ryoo, M. Kruk, M. Jaroniec, Z. Liu, T. Ohsuna, O. Terasaki, Synthesis of new, nanoporous carbon with hexagonally ordered mesostructure, J. Am. Chem. Soc. 122 (43) (2000) 10712–10713.

[17] J. Roggenbuck, H. Schäfer, T. Tsoncheva, C. Minchev, J. Hanss, M. Tiemann, Mesoporous CeO_2: Synthesis by nanocasting, characterisation and catalytic properties, Microporous Mesoporous Mater. 101 (3) (2007) 335–341.

[18] G. Kresse, Ab initio molecular dynamics for liquid metals, J. Non. Cryst. Solids 192-193 (1995) 222–229.

[19] J. Hafner, Ab-initio simulations of materials using VASP: density-functional theory and beyond, J. Comput. Chem. 29 (2008) 2044–2078.

[20] J.P. Perdew, K. Burke, M. Ernzerhof, Generalized gradient approximation made simple, Phys. Rev. Lett. 77 (18) (1996) 3865–3868.

[21] H.J. Monkhorst, J.D. Pack, Special points for brillouin-zone integrations, *Phys. Rev. B - Condens. Matter Mater. Phys.* 13 (12) (1976) 5188–5192.

[22] G. Kresse, D. Joubert, From ultrasoft pseudopotentials to the projector augmented-wave method, *Phys. Rev. B - Condens. Matter Mater. Phys.* 59 (3) (1999) 11–19.

[23] G. Henkelman, A. Arnaldsson, H. Jonsson, A fast and robust algorithm for Bader decomposition of charge density, Comput. Mater. Sci. 36 (2006) 354–360.

[24] J. Zaffran, M. Caspary, Metal – oxygen bond Ionicity as an efficient descriptor for doped NiOOH photocatalytic activity, ChemPhysChem 17 (2016) 1630–1636.

[25] J. Zaffran, M.C. Toroker, Benchmarking density functional theoy based methods to model NiOOH material properties : Hubbard and Van der Waals corrections vs . hybrid Functionals, J. Chem. Theory Comput. 12 (8) (2016) 3807–3812.

[26] J. Zaffran, M.B. Stevens, C.D.M. Trang, M. Shehadéh, S.W. Boettcher, M. C. Toroker, Influence of electrolyte cations on Ni (Fe) OOH catalyzed oxygen evolution reaction, Chem. Mater. 29 (11) (2017) 4761–4767.

[27] H.A. Evans, R. Seshadri, A.K. Cheetham, Perovskite-related ReO3-type structures, Nat. Rev. Mater. 5 (1) (2020) 196–213.

[28] V.K. Meisel, Uber die kristallstrucktur des Rheniumtrioxyds, Zeitschrift fur Anorg. und Allg. Chemie 207 (1) (1932) 121–128.

[29] J.P. Suchitra, U.V Waghmare, principles analysis High tunability of the work function of (001) surface of ReO_3 with O-vacancies : First principles analysis, J. Appl. Phys. 116 (2014), 034304.

[30] J. Okal, W. Tylus, L. Kępiński, XPS study of oxidation of rhenium metal on γ-Al_2O_3 support, J. Catal. 225 (2) (2004) 498–509.

[31] W.T. Tysoe, F. Zaera, G.A. Somorjai, An XPS study of the oxidation and reduction of the rhenium-platinum system under atmospheric conditions, Surf. Sci. 200 (1) (1988) 1–14.

[32] L. Fiorani, M. Passacantando, S. Santucci, S. Di Marco, S. Bisti, R. Maccarone, Cerium oxide nanoparticles reduce microglial activation and neurodegenerative events in light damaged retina, PLoS One 10 (10) (2015) 1–18.

[33] W. Shan, H. Guo, C. Liu, X. Wang, Controllable preparation of CeO_2 nanostructure materials and their catalytic activity, J. Rare Earths 30 (7) (2012) 665–669.

[34] C. Ho, J.C. Yu, T. Kwong, A.C. Mak, S. Lai, Morphology-controllable synthesis of mesoporous CeO_2 nano- and microstructures, Chem. Mater. 17 (17) (2005) 4514–4522.

[35] W. Ahmed, A.E. Awadallah, A.A. Aboul-Enein, Ni/CeO_2–Al_2O_3 catalysts for methane thermo-catalytic decomposition to CO_x-free H_2 production, Int. J. Hydrogen Energy 41 (41) (2016) 18484–18493.

[36] N. Ota, M. Tamura, Y. Nakagawa, K. Okumura, K. Tomishige, Performance, structure, and mechanism of ReO_x-Pd/CeO_2 catalyst for simultaneous removal of vicinal OH groups with H_2, ACS Catal 6 (5) (2016) 3213–3226.

[37] S. Vorakitkanvasin, S.K.N. Ayudhya, K. Suriye, P. Praserthdam, J. Panpranot, Enhanced metathesis activity of low loading Re_2O_7/Al_2O_3 catalysts for propylene production by using aluminum nitrate as Al_2O_3 precursor, Appl. Catal. A Gen. 517 (2016) 39–46.

[38] L. Sang, S. Chen, G. Yuan, M. Zheng, J. You, A. Chen, R. Li, L. Chen, Metathesis of 1-butene and 2-butene to propene over Re_2O_7 supported on macro-mesoporous γ-alumina prepared via a dual template method, J. Nat. Gas Chem. 21 (2) (2012) 105–108.

[39] M. Boaro, M. Vicario, C. De Leitenburg, G. Dolcetti, A. Trovarelli, The use of temperature-programmed and dynamic/transient methods in catalysis: Characterization of ceria-based, model three-way catalysts, Catal. Today 77 (4) (2003) 407–417.

[40] J.M. De Souza e Silva, M. Strauss, C.M. Maroneze, E.R. Souza, Y. Gushikem, F. A. Sigoli, I.O. Mazali, Synthesis and structural characterization of nanometric ceria highly dispersed in SBA-15 with oxygen exchange capacity, J. Mater. Chem. 21 (39) (2011) 15678–15685.

[41] J.H. Jang, H. Sohn, J. Camacho-Bunquin, D. Yang, C. Park, M. Delferro, M. Abu-Omar, Deoxydehydration of biomass-derived polyols with a reusable unsupported rhenium nanoparticles catalyst, ACS Sustain. Chem. Eng. 7 (13) (2019) 11438–11447.

[42] M.T. Greiner, T.C.R. Rocha, B. Johnson, A. Klyushin, A. Knop-Gericke, R. Schlögl, The oxidation of rhenium and identification of rhenium oxides during catalytic partial oxidation of ethylene: An in-situ xps study, Zeitschrift fur Phys. Chemie 228 (4–5) (2014) 521–541.

[43] L. Liu, T. Asano, Y. Nakagawa, M. Tamura, K. Okumura, K. Tomishige, Selective hydrogenolysis of glycerol to 1,3-Propanediol over Rhenium-Oxide-modified iridium nanoparticles coating Rutile Titania support, ACS Catal 9 (2019) 10913–10930.

[44] M. Lupacchini, A. Mascitti, V. Canale, L. Tonucci, E. Colacino, M. Passacantando, A. Marrone, N. D'Alessandro, Deoxydehydration of glycerol in presence of rhenium compounds: Reactivity and mechanistic aspects, Catal. Sci. Technol. 9 (12) (2019) 3036–3046.

[45] H. Hayasaka, S. Tazawa, N. Ota, Y. Nakagawa, and K. Tomishige, "Deoxydehydration of Glycerol to Allyl Alcohol over ReOx -Au /CeO2 catalyst with," pp. 5–6.

[46] T. Wang, X. Yuan, S. Li, L. Zeng, J. Gong, CeO_2-modified Au@SBA-15 nanocatalysts for liquid-phase selective oxidation of benzyl alcohol, Nanoscale 7 (17) (2015) 7593–7602.

[47] Y. Dong, J. Luo, S. Li, C. Liang, CeO2 decorated Au/CNT catalyst with constructed Au-CeO_2 interfaces for benzyl alcohol oxidation, Catal. Commun. 133 (August 2019) (2020) 1–5.

[48] D. Zhang, X. Du, L. Shi, R. Gao, Shape-controlled synthesis and catalytic application of ceria nanomaterials, Dalt. Trans. 41 (48) (2012) 14455–14475.

[49] X. Huang, K. Zhang, B. Peng, G. Wang, M. Muhler, F. Wang, Ceria-based materials for Thermocatalytic and photocatalytic organic synthesis, ACS Catal 11 (15) (2021) 9618–9678.

[50] C. Pischetola, L. Collado, M.A. Keane, F. Cárdenas-Lizana, Gas phase hydrogenation of furaldehydes via coupling with alcohol dehydrogenation over ceria supported Au-Cu, Molecules 23 (11) (2018) 1–16.

[51] D.R. Mullins, S.D. Senanayake, T.L. Chen, Adsorption and reaction of C1-C3 alcohols over CeO_X(111) thin films, J. Phys. Chem. C 114 (40) (2010) 17112–17119.

[52] A. Beste, S.H. Overbury, Pathways for ethanol dehydrogenation and dehydration catalyzed by ceria (111) and (100) surfaces, J. Phys. Chem. C 119 (5) (2015) 2447–2455.

[53] J. Yi, J. Miller, D. Zemlyanov, R. Zhang, P. Dietrich, F. Ribeiro, S. Suslov, M. Abu-Omar, A reusable unsupported rhenium nanocrystalline catalyst for acceptorless dehydrogenation of alcohols through γ-C-H activation, Angew. Chemie 126 (3) (2014) 852–855.

[54] Y. Nakagawa, S. Tazawa, T. Wang, M. Tamura, N. Hiyoshi, K. Okumura, K. Tomishige, Mechanistic study of hydrogen-driven Deoxydehydration over Ceria-supported rhenium catalyst promoted by Au nanoparticles, ACS Catal 8 (1) (2018) 584–595.

[55] N.N. Tshibalonza, J.C.M. Monbaliu, The deoxydehydration (DODH) reaction: a versatile technology for accessing olefins from bio-based polyols, Green Chem 22 (15) (2020) 4801–4848.

[56] J. Zaffran, M. Caspary, Designing efficient doped NiOOH catalysts for water splitting with first principles calculations, ChemistrySelect 5 (2016) 911–916.

[57] C. Michel, F. Auneau, Linear energy relations as predictive tools for polyalcohol catalytic reactivity, ACS Catal 4 (2014) 464–468.

[58] P. Sautet, C. Michel, Trade-off between accuracy and universality in linear energy relations for alcohol dehydrogenation on transition metals, J. Phys. Chem. (2015).